Surface-enhanced magneto-optics in metallic multilayer films

C. Hermann, V. A. Kosobukin,* G. Lampel, J. Peretti, V. I. Safarov,† and P. Bertrand

Laboratoire de Physique de la Matière Condensée (CNRS-UMR/C 7643), Ecole Polytechnique, 91128 Palaiseau Cedex, France
(Received 24 April 2001; published 29 November 2001)

The magneto-optical properties of noble-metal–ferromagnetic-metal multilayer thin films have been investigated as a function of the incidence angle, including the total reflection range, in the polar, longitudinal, and equatorial geometries, and for different values of the photon energy in the near-infrared and visible spectrum. The experimental and theoretical results are obtained on a Au/Co/Au model system. They demonstrate that the resonant coupling of the *p* component of the light electric field with the gold surface plasmon, which occurs in the total reflection range, yields a strong enhancement of the magneto-optical response and signal-to-noise ratio of the system for the three magnetization directions. This resonant coupling and the resulting enhancement of the relevant magneto-optical quantities are achieved for any photon energy in the near infrared and visible range simply by tuning the incidence angle. The efficiency of this enhancement effect is shown to increase towards the infrared region of the spectrum following the rise of the quality factor of the surface plasmon resonance.

I. INTRODUCTION

The enhancement of magneto-optical (MO) effects stimulates a wide interest as it may promote new capabilities of optical techniques for studying magnetic material properties and because of the possible applications to information storage. Several approaches are proposed apart from the elaboration of magnetic materials with high MO constants. They are mainly based on the design of a multilayer structure which exhibits an optimized MO figure of merit for a given magnetic material in a given light energy range. The structure can be the combination of an active material either with dielectric layers[1] or with nonmagnetic metal layers.[2,3] For instance, it has been shown that ferromagnetic-metal–noble-metal multilayer structures exhibit increased Kerr rotation at the plasma edge of the noble metal matrix dielectric function ε.[2] Nevertheless, the MO response and figure of merit of these structures are not necessarily enhanced because of the losses and a low reflectivity.[3]

However, it has been shown that a resonant electromagnetic mechanism, similar to those which provide surface-enhanced Raman scattering and related phenomena,[4] does exist for improving the MO response and figure of merit of noble-metal–ferromagnetic-metal multilayer thin films.[5,6] This mechanism involves the metal surface plasmon (SP) modes[7–9] which can be excited, in a wide spectral range, by the *p* component of the evanescent light electric field propagating along the surface of a thin metallic film illuminated in total reflection condition. An early work reporting on the influence of SP's on Kerr effect only concerned pure ferromagnetic metal thin films,[10] where the SP's are not well defined due to overdamping ($|\text{Re}(\varepsilon_m)/\text{Im}(\varepsilon_m)|<1$, ε_m being the magnetic metal dielectric function). In this case, the Kerr rotation is large but the figure of merit is in fact not enhanced. In comparison, noble-metal–ferromagnetic-metal multilayer thin films provide a significant advantage as the quality factor of the noble metal SP resonance is high ($|\text{Re}(\varepsilon)/\text{Im}(\varepsilon)|\gg1$).

In the present paper, we report a detailed and complete experimental and theoretical study of the MO properties, in total reflection geometry, of a model Au/Co/Au structure. In this system, the easy-magnetization direction of the Co layer can be chosen either perpendicular or parallel to the film plane simply by changing the thickness of the Co layer. This allows one to study the three different Kerr geometries in almost identical systems. As we have already demonstrated in the case of the polar configuration,[5] our results show that a resonance characteristic feature is observed in Kerr effects, for the three magnetization directions, when the gold SP's are excited. This feature corresponds to a strong enhancement of the MO response, figure of merit and signal-to-noise ratio of the whole system. The resonant coupling of light with the SP modes and the resulting enhancement of these relevant MO quantities are achieved for any photon energy in the near infrared and visible spectra, simply by tuning the incidence angle. In the infrared range, as the quality factor of the SP resonance increases, the resonant feature of the MO response becomes sharper and the enhancement effect more efficient.

In Sec. II, we give the basic principles and a theoretical description of surface enhanced magneto-optics in noble-metal–ferromagnetic-metal multilayer systems. In Sec. III, we describe the characteristics of our Au/Co/Au samples, the experimental setup, and the procedure used for measuring the MO effects. In Sec. IV, we present and discuss the experimental results obtained for the different magnetization directions and for various light excitation energies.

II. PRINCIPLE AND THEORY

A. Surface plasmon modes in noble metals

The characteristics of metal SP modes are well established.[7–9] These coherent charge oscillations propagate along the metal surface and they may couple with photons in the total reflection geometry. The commonly used experimental arrangement is the Kretschmann-Raether configuration:[11] a parallel slab of metal (medium 2 of dielectric function $\varepsilon_2 = \varepsilon_2' + i\varepsilon_2''$), with one face in contact with air

64 235422-1

(medium 3 of dielectric function ε_3), is illuminated at an incidence angle θ through a glass prism (medium 1 of dielectric function $\varepsilon_1 = n_1^2$). The incidence plane is xOz, the interface plane is xOy and **x**, **y**, and **z** are the unit vectors of the Ox, Oy, and Oz axes. After Snell-Descartes law, the photon wave-vector component q, in the interface plane (along Ox), is conserved through the structure.

In this geometry, photons illuminating the metal surface are described by the dispersion relation

$$\omega = \frac{cq}{n_1 \sin \theta_1} \qquad (1)$$

where ω and c are respectively the pulsation and velocity of light in vacuum.

In medium i, the light wave vector is $\mathbf{k}_i = q\mathbf{x} + \kappa_i \mathbf{z}$, and κ_i is related to the dielectric constant ε_i by

$$\mathbf{k}_i^2 = \varepsilon_i k_0^2 = q^2 + \kappa_i^2, \qquad (2)$$

where $k_0 = \omega/c$.

For an α-polarized wave, where α stands for s or p (respectively **E** or **B** normal to the incidence plane), the coefficients of reflection r_{ij}^{α} and transmission t_{ij}^{α} at a plane interface between media i and j are derived from the conservation of the in-plane components of **E** and **B**:[12]

$$r_{ij}^{\alpha} = \frac{a_i^{\alpha} - a_j^{\alpha}}{a_i^{\alpha} + a_j^{\alpha}}, \qquad t_{ij}^{\alpha} = \frac{2\gamma_{ij}^{\alpha} a_i^{\alpha}}{a_i^{\alpha} + a_j^{\alpha}}, \qquad (3)$$

where $a_i^s = \kappa_i/k_0$, $a_i^p = -\kappa_i/(k_0\varepsilon_i)$, $\gamma_{ij}^s = 1$, and $\gamma_{ij}^p = n_i/n_j$.

For a p-polarized excitation, a particular situation may occur at the metal-air interface when $a_2^p + a_3^p \approx 0$, that is,

$$\kappa_2/\varepsilon_2 \approx -\kappa_3/\varepsilon_3. \qquad (4)$$

This condition, equivalent to the existence condition of SP's,[9] can be fulfilled in a noble metal below the bulk plasmon pulsation, when $\varepsilon_2 \approx \varepsilon_2'(|\varepsilon_2'| \gg \varepsilon_2'')$ and $\varepsilon_2' \ll -1$. Thus, κ_3 is imaginary and κ_2 mostly imaginary so that the light wave which couples with the SP's is evanescent in medium 3. This results in a strong enhancement of r_{23}^p and t_{23}^p which at resonance become large and imaginary: $t_{23}^p \approx r_{23}^p \approx -4i\varepsilon_2'/\varepsilon_2''$.

Equation (4) combined with Eq. (2) yields the dispersion relation of SP's, as schematized in Fig. 1:

$$\omega = cq \left(\frac{\varepsilon_2' + \varepsilon_3}{\varepsilon_2' \varepsilon_3} \right)^{1/2}. \qquad (5)$$

By comparison with Eq. (1), the photon and SP dispersion relations intercept for a value θ_R of the incidence angle in medium 1 given by

$$\sin \theta_R = \frac{n_3}{n_1} \left(\frac{\varepsilon_2'}{\varepsilon_2' + \varepsilon_3} \right)^{1/2}. \qquad (6)$$

This condition can be fulfilled only if $n_1 > n_3$, as expected since the SP excitation requires a total internal reflection geometry (κ_3 imaginary).
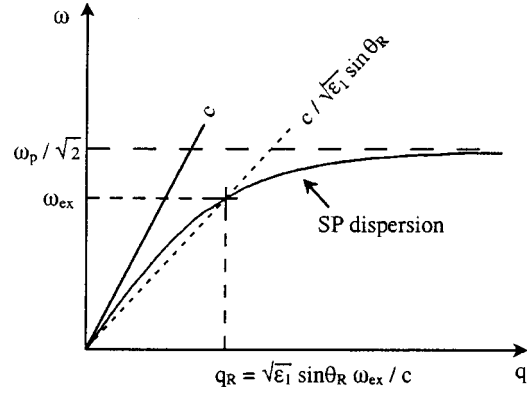
FIG. 1. Schematic plot of the dispersion relation of surface plasmons taking into account the $\varepsilon_2(\omega)$ dispersion relation. The dispersion relation of light (pulsation ω as a function of q, the wave vector component parallel to the surface) is plotted for illumination of the metallic surface from the vacuum side in grazing incidence (straight line of slope c, the light velocity in vacuum) and for illumination through a prism of dielectric constant ε_1 at an angle of incidence θ_R larger than θ_c [dotted line of slope $c/\sqrt{\varepsilon_1} \sin \theta_R$]. In this latter geometry, the coupling of photons with surface plasmons is possible and occurs in the illumination conditions corresponding to the interception of their dispersion curves.

The resonance is generally evidenced by measuring the reflectivity as a function of the incidence angle in the total reflection range. For an α-polarized incident wave, the amplitude reflection coefficient in medium 1 is given by

$$R_{\text{Au}}^{\alpha} = \frac{r_{12}^{\alpha} + r_{23}^{\alpha} \exp(2i\kappa_2 d)}{1 - r_{12}^{\alpha} r_{23}^{\alpha} \exp(2i\kappa_2 d)}. \qquad (7)$$

For p-polarized incident light, the reflectivity $|R_{\text{Au}}^p|^2$ exhibits a dip,[7] corresponding to the minimum of the numerator occurring in the SP region.

At the distance z from the prism/metal interface, the fields inside the metal layer are, respectively, given, for s- and p-polarized incident waves of unit amplitude, by

$$\mathbf{e}_{21}^s = t_{12}^s \exp(i\kappa_2 z) \frac{1 + r_{23}^s \exp[2i\kappa_2(d-z)]}{1 - r_{12}^s r_{23}^s \exp(2i\kappa_2 d)} \mathbf{y}, \qquad (8a)$$

$$\mathbf{e}_{21}^p(z) = t_{12}^p \exp(i\kappa_2 z) \left[\frac{1 - r_{23}^p \exp[2i\kappa_2(d-z)]}{1 - r_{12}^p r_{23}^p \exp(2i\kappa_2 d)} \frac{\kappa_2}{k_2} \mathbf{x} \right.$$
$$\left. + \frac{1 + r_{23}^p \exp[2i\kappa_2(d-z)]}{1 - r_{12}^p r_{23}^p \exp(2i\kappa_2 d)} \frac{q}{k_2} \mathbf{z} \right]. \qquad (8b)$$

In the case of a 30-nm-thick gold film illuminated with a light of wavelength 633 nm, the variations of e_{21}^s and e_{21}^p versus z are shown in Fig. 2 for two incidence angles: below the total reflection critical angle θ_c and at the resonance angle θ_R. When the SP resonance is not excited (for p polarization when $\theta \neq \theta_R$ and for s polarization), $|r_{23}^{\alpha}|$ is smaller than unity so that the field components decrease with z almost as $\exp(i\kappa_2 d)$ (κ_2 is mainly imaginary). At resonance where $|r_{23}^p|$ is larger than 1, the x and z components of $\mathbf{e}_{21}^p(z)$, $e_{21}^x(z)$, and $e_{21}^z(z)$ are strongly enhanced. They almost in-
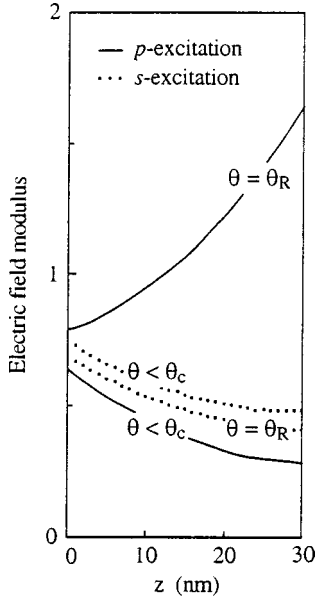
FIG. 2. Variation with the distance z to the prism/metal interface of the light electric field modulus inside of the noble metal layer for unit s and p excitations and for two values of the incidence angle: one lower than θ_c, the other θ_R corresponding to the resonant excitation of the noble metal surface plasmons.

crease with z as $\exp(-i\kappa_2 d)$, that is they are maximum at the gold-air interface where the SP resonance takes place.

The mechanism that we propose here for the enhancement of the MO effects is then based on the assumption that a thin magnetic layer inserted in the noble metal film is exposed to a strong field at resonance and one can therefore expect a related enhancement of the MO response of this layer.

B. First-order MO effects in metallic multilayer thin films

The system under study is a thin ferromagnetic (cobalt) layer of thickness ℓ, sandwiched between two noble metal (gold) layers, the upper one of thickness d' deposited on the glass prism and the lower one of thickness d'' deposited on the top of the magnetic layer (inset in Fig. 3). The structure is illuminated through the prism at an incidence angle θ_ℓ by a β-polarized plane wave (where β stands for s or p) of pulsation ω.

For any homogeneous magnetization $\mathbf{M}$, the material equation in the cobalt layer relating the displacement vector $\mathbf{D}_m(z)$ to the electric field $\mathbf{E}_m(z)$ is

$$\mathbf{D}_m(z) = \varepsilon_0 \varepsilon_m \mathbf{E}_m(z) + \varepsilon_0 g \mathbf{M} \wedge \mathbf{E}_m(z). \tag{9}$$

The term $\varepsilon_0 \varepsilon_m \mathbf{E}_m(z)$ describes the isotropic response of the material and, as discussed in Chap. IV of Ref. 12, $\varepsilon_0 g \mathbf{M} \wedge \mathbf{E}_m(z)$ represents an induced radiating electric polarization. The quantity g is a MO characteristic constant and gM is always small relatively to ε_m. Therefore, $\mathbf{E}_m(z)$ can be approximated, to first order in gM and for an excitation wave of unit amplitude incident from medium 1, by the unperturbed field in the cobalt layer $\mathbf{e}_{m1}^{0\beta}(z)$ calculated for zero magnetization (first Born approximation).
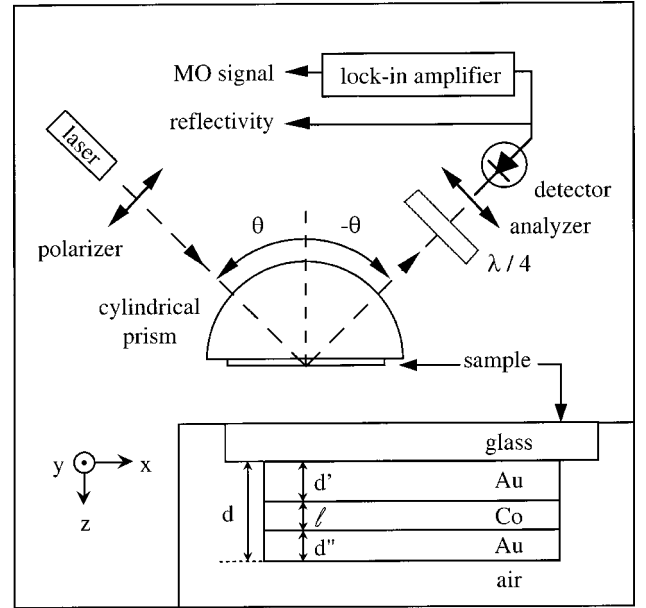
FIG. 3. Schematics of the magneto-optics experimental setup. The inset shows the sample composition.

Within this approximation and for a thin layer ($|\kappa_m \ell| \ll 1$) where $\mathbf{e}_{m1}^{0\beta}(z)$ is almost a constant $\mathbf{e}_{m1}^{0\beta}$, the MO α-polarized component of the reflected wave is given by[12]

$$\Delta R^{\alpha\beta} = \frac{-ik_0^2 \ell}{2\kappa_1} g\mathbf{M}(\overline{\mathbf{e}}_{m1}^{0\alpha} \wedge \mathbf{e}_{m1}^{0\beta}). \tag{10}$$

In this equation, $\overline{\mathbf{e}}_{m1}^{0\alpha}$, the extraction vector of the α-polarized field radiated by the MO induced electrical polarization, is the symmetric of $\mathbf{e}_{m1}^{0\alpha}$ with respect to the yOz plane. This expression is valid for any magnetization direction, incident polarization β and incident angle.

C. Gold SP resonance feature in the MO response

The magneto-optical effects are given in Eq. (10) as a function of the unperturbed fields $\mathbf{e}_{m1}^{0\beta}$ and $\overline{\mathbf{e}}_{m1}^{-0\alpha}$ in the cobalt layer. However, as discussed in Chap. VI of Ref. 12 and in the Appendix, since the cobalt layer is thin, these fields can be related by a perturbation method to the fields $\mathbf{e}_{21}^{\beta}$ and $\overline{\mathbf{e}}_{21}^{\alpha}$ in a pure gold layer of thickness d equal to the total thickness of the Au/Co/Au sandwich ($d = d' + \ell + d''$):[12]

$$\mathbf{e}_{m1}^{0\alpha} = \frac{\mathbf{e}_{21}^{\alpha}(z_c)}{1 - \delta T^{\alpha}/T_{\text{Au}}^{\alpha}}. \tag{11}$$

Here, the altitude z_c in the equivalent gold layer represents the distance between the glass-gold interface and the center of the cobalt layer, T_{Au}^{α} is the complex transmission coefficient of the pure gold equivalent layer, and δT^{α} is the first-order perturbation of the transmission due to the cobalt layer (see the Appendix).

The MO reflection coefficients of the gold-cobalt-gold sandwich can thus be written as a function of the fields in the equivalent gold layer

$$\Delta R^{\alpha\beta} \sim \frac{-ik_0^2 \ell}{2\kappa_1} \frac{g\mathbf{M}[\overline{\mathbf{e}}_{21}^{\alpha}(z_c) \wedge \mathbf{e}_{21}^{\beta}(z_c)]}{(1-\delta T^{\alpha}/T_{\mathrm{Au}}^{\alpha})(1-\delta T^{\beta}/T_{\mathrm{Au}}^{\beta})}. \quad (12)$$

Therefore, the MO quantity $\Delta R^{\alpha\beta}$ exhibits the SP resonant feature of $\mathbf{e}_{21}^p$ and/or $\overline{\mathbf{e}}_{21}^p$, the p fields in the equivalent gold layer. The damping due to the losses in the Co layer, described by $\delta T^{s,p}/T_{\mathrm{Au}}^{s,p}$, can be shown to be small for the Co layer thicknesses used in the present experimental study (see the Appendix) so that the gold SP enhancement effect, originating from $\overline{\mathbf{e}}_{21}^p$ and/or $\overline{\mathbf{e}}_{21}^p$, remains.

For $\mathbf{M}$ along Oz, the magneto-optical coefficients are

$$\Delta R^{ps} = \Delta R^{sp} \approx \frac{ik_0^2 \ell}{2\kappa_1} \frac{gM^z e_{21}^y(z_c) e_{21}^x(z_c)}{(1-\delta T^s/T_{\mathrm{Au}}^s)(1-\delta T^p/T_{\mathrm{au}}^p)}. \quad (13)$$

For $\mathbf{M}$ along Ox, we derive

$$\Delta R^{ps} = -\Delta R^{sp} \approx \frac{ik_0^2 \ell}{2\kappa_1} \frac{gM^x e_{21}^y(z_c) e_{21}^z(z_c)}{(1-\delta T^s/T_{\mathrm{Au}}^s)(1-\delta T^p/T_{\mathrm{Au}}^p)}. \quad (14)$$

In Eqs. (13) and (14), the enhancement of $\Delta R^{\alpha\beta}$ due to the SP resonance respectively arise from $e_{21}^x(z_c)$ and $e_{21}^z(z_c)$. The same enhancement effect occurs for both s- and p-polarized incident lights: for a p-polarized incident wave, the exciting field is enhanced and induces a large electric polarization which in turn radiates; for a s-polarized incident wave, the induced MO electric polarization radiates p-polarized waves enhanced by the SP resonance.

Finally, for $\mathbf{M}$ along Oy, there is no s-p coupling ($\Delta R^{sp} = \Delta R^{ps} = 0$), but a modification ΔR^{pp} of the p-wave reflection coefficient R^{pp}:

$$\Delta R^{pp} \approx \frac{ik_0^2 \ell}{2\kappa_1} \frac{gM^y e_{21}^z(z_c) e_{21}^x(z_c)}{(1-\delta T^p/T_{\mathrm{Au}}^p)^2}. \quad (15)$$

Here, the SP resonance enhances both the exciting field and the field radiated by the induced MO polarization.

III. EXPERIMENTAL

A. The Au/Co/Au samples

In a Au/Co/Au sandwich structure, the easy-magnetization direction changes with the thickness of the cobalt layer from perpendicular to in-plane configuration. This allowed us to study the three (polar, longitudinal, and equatorial) Kerr effects with two very similar samples.

The first specimen (sample 1) of total thickness $d = 30$ nm, where the $\ell = 1$-nm-thick cobalt layer has its easy-magnetization axis perpendicular to the film plane, was used for the polar Kerr experiments. The thicknesses of the under and cap gold layers are, respectively, $d' = 25$ nm and $d'' = 4$ nm. The second specimen (sample 2), for which $d = 35.7$ nm, $d' = 24.2$ nm, $d'' = 5.8$ nm, and $\ell = 5.7$ nm, exhibits an in-plane easy-magnetization axis and was studied in the longitudinal and equatorial Kerr geometries. Both samples were grown on a float glass substrate under UHV conditions and exhibit a square hysteresis loop.[13]
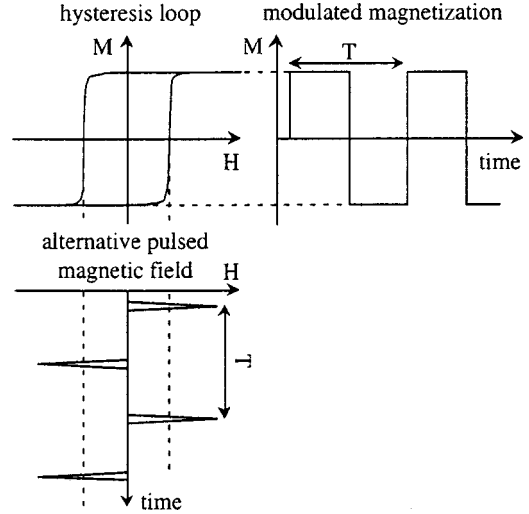
FIG. 4. Principle of the MO effects measurements by alternating pulsed magnetic field modulation technique. Short (≈ 10 μs long) alternating pulses of magnetic field larger than the Co-layer coercive field (≈ 800 Oe for sample 1 and ≈ 200 Oe for sample 2) are applied at a low repetition rate ($1/\tau \approx 20$ Hz). Consequently, the saturated magnetization of the Co layer is periodically flipped.

B. The experimental setup and procedure

In our experiment (Fig. 3), the glass substrate, of dielectric constant $\varepsilon_1 = 2.28$, is optically coupled to a half-cylindrical glass prism by an adapting refractive index liquid. Linearly polarized light emitted from a Krypton-ion laser illuminates the sample through the prism at a variable incident angle θ. A $\lambda/2$-retardation plate, when rotated by $45°$, allows us to change the incident polarization from s to p. The intensity and the polarization state of the reflected beam are analyzed.

The Kerr effects are measured by means of specific modulation techniques. A small magnetic coil is set near the sample surface with its axis parallel to the Co-layer easy-magnetization axis (along the z direction for polar Kerr measurements on sample 1 and along the x and y directions for, respectively, longitudinal and equatorial MO experiments on sample 2). As described in Fig. 4, under alternative pulsed current operation of the coil the saturated magnetization of the Co layer is periodically flipped. For polar and longitudinal geometries the resulting modulation of the reflected light polarization induced by the MO effect is detected as an intensity modulation through a polarization analyzer. This analyzer is either a linear analyzer oriented at $45°$ to the incident polarization axis, or a circular analyzer, i.e., a quarter-wave plate inserted after the linear analyzer which is oriented at $45°$ from the retarding plate axis. In the equatorial geometry the MO effect directly induces a modulation of the reflected p intensity and we have performed the MO measurements first without analyzer as is usually done, and then in a particular configuration that we will detail further. In the three Kerr geometries, the ac component of the detector output signal at the modulation frequency, measured through a lock-in amplifier, is the amplitude of the MO hysteresis loop at zero external magnetic field. For a unit excitation intensity,
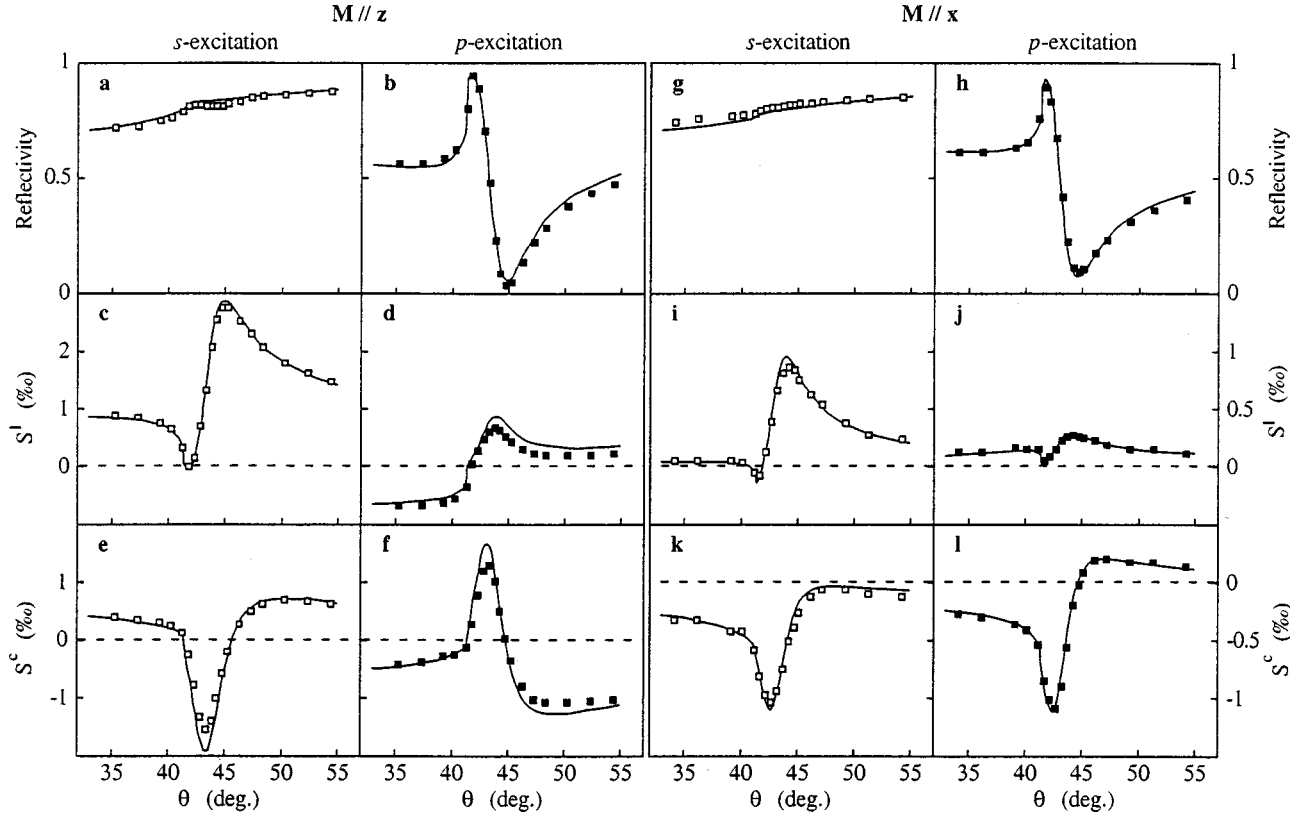
FIG. 5. Variation with the incidence angle θ of the reflectivity (curves a,b and g,h) and of the polar (**M**||**z**) (curves c–f) and longitudinal (**M**||**x**) (curves i–l) MO response S of the Au/Co/Au samples. The left columns (curves a,c,e and g,i,k) correspond to s excitation and the right column (curves b,d,f and h,j,l) to p excitation. The MO signal is measured in the reflected beam with a linear-light analyzer (curves c,d and i,j) and with a circular-light analyzer (curves e,f and k,l). The symbols correspond to the experimental data and the full lines represent the theoretical fits.

the dc detector output signal yields the reflected intensity $\mathcal{R}_I$ and the ac signal is the MO response S of the system.

IV. RESULTS AND DISCUSSION

A. Effect of the SP resonance on the MO response for the different Kerr geometries

1. Polar and longitudinal MO effects

In the polar (**M**||**x**) and longitudinal (**M**||**z**) geometries, the MO effect induces a component perpendicular to the incident polarization direction. Therefore, whatever the excitation polarization β, the reflected light electric field is the sum of a β component of amplitude $R^{0\beta}$ and of the MO α-polarized component of amplitude $\Delta R^{\alpha\beta}(\alpha \neq \beta)$. The expressions of the different quantities that we measure, the reflectivity $\mathcal{R}_I$ and the MO signals S^l and S^c, respectively with a linear and a circular analyzer, are then

$$\mathcal{R}_I = |R^{0\beta}|^2 + |\Delta R^{\alpha\beta}|^2 \approx |R^{0\beta}|^2, \quad (16)$$

$$S^l = 2|R^{0\beta}||\Delta R^{\alpha\beta}|\cos(\Delta\phi^{\alpha\beta}) \quad \text{and}$$

$$S^c = 2|R^{0\beta}||\Delta R^{\alpha\beta}|\sin(\Delta\phi^{\alpha\beta}), \quad (17)$$

where $\Delta\phi^{\alpha\beta}$ is the phase difference between $|R^{0\beta}|$ and $|\Delta R^{\alpha\beta}|$. Thus, with the measurements of $\mathcal{R}_I$, S^l, and S^c, for

each incident polarization β (s and p), the three physical quantities which determine the MO response of the system, namely, $|R^{0\beta}|$, $|\Delta R^{\alpha\beta}|$, and $\Delta\phi^{\alpha\beta}$, can be obtained.

We have performed the measurements of $\mathcal{R}_I$, S^l, and S^c as a function of the incidence angle, in the polar and longitudinal geometries (respectively, on sample 1 and sample 2), for s and p excitations, with a light wavelength $\lambda = 647$ nm. The results are presented in Fig. 5. The symbols represent the experimental data and the full lines are obtained after the theoretical treatment presented in Sec. II C and in the Appendix. The values of the dielectric constants used in this calculation ($\varepsilon_2 = -11 + 2i$, $\varepsilon_m = -11.5 + 18.3i$, $gM_z = -0.6488 + 0.0007i$, and $gM_x = gM_y = -0.5725 - 0.1045i$) are close to those generally quoted in the literature.[14–16] In both configurations, the results are very similar.

For p excitation, the pronounced minimum of reflectivity (Fig. 5, curves b and h) characteristic of the excitation of the gold SP's is observed at the resonance angle $\theta_R \approx 44.5°$ beyond the total reflection critical angle θ_c ($\approx 41.5°$ in the present case). As shown in the Appendix, because of the presence of the Co layer, the width of this peak is larger than in a pure gold film and this broadening is more important for sample 2 ($\ell = 5.7$ nm) than for sample 1 ($\ell = 1$ nm). In the MO responses S^l and S^c, a remarkable feature is observed around θ_R for both s and p excitations.

Straightforwardly deduced with Eqs. (16) and (17) from the measurements, the resonant character of this feature is
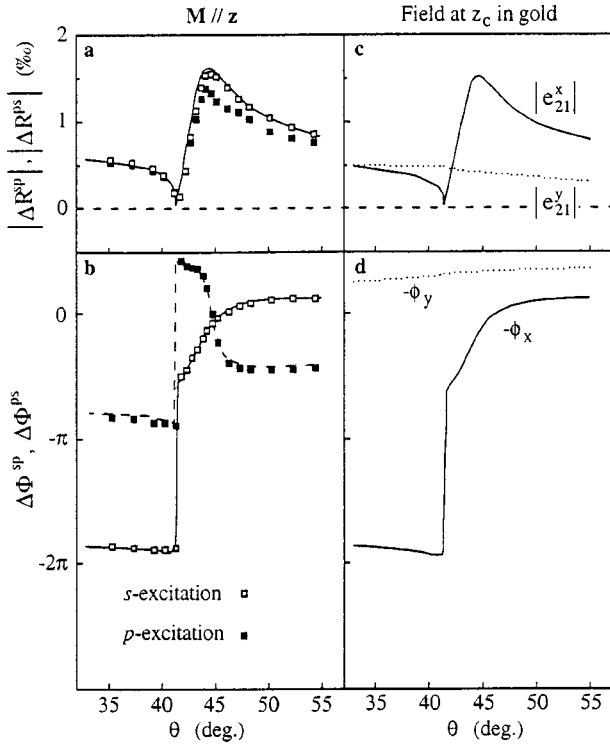
FIG. 6. Variation with the incidence angle θ of the polar ($\mathbf{M}\|\mathbf{z}$) MO reflection coefficients, measured on sample 1, for s and p excitations: the moduli $|\Delta R^{ps}|$ and $|\Delta R^{sp}|$ (curve a) and the phase differences $\Delta\Phi^{ps}$ and $\Delta\Phi^{sp}$ (curves b) are deduced from the data presented in Fig. 5. The symbols correspond to the measurements, the full and dotted lines represent the theoretical fits (which are identical for $|\Delta R^{ps}|$ and $|\Delta R^{sp}|$). The experimental data can be compared with the modulus (curves c) and phase (curves d) of the x and y components of the excitation field calculated in a pure gold film at the location of the Co layer center.

FIG. 7. Variation with the incidence angle θ of the longitudinal ($\mathbf{M}\|\mathbf{x}$) MO reflection coefficients, measured on sample 2, for s and p excitations: the moduli $|\Delta R^{ps}|$ and $|\Delta R^{sp}|$ (curves a) and the phase differences $\Delta\Phi^{ps}$ and $\Delta\Phi^{sp}$ (curves b) are deduced from the data presented in Fig. 5. The symbols correspond to the measurements, the full and dotted lines represent the theoretical fits (which are identical for $|\Delta R^{ps}|$ and $|\Delta R^{sp}|$). The experimental data can be compared with the modulus (curves c) and phase (curves d) of the z and y components of the excitation field calculated in a pure gold film at the location of the Co layer center.

evidenced when considering the variations with θ of the MO component of the reflected light electric field $\Delta R^{\alpha\beta}$, i.e., of the related MO quantities $|\Delta R^{\alpha\beta}|$ and $\Delta\phi^{\alpha\beta}$ [curves (a) and (b) in Figs. 6 and 7 for, respectively, polar and longitudinal geometries]. For both polar and longitudinal geometries, the moduli $|\Delta R^{\alpha\beta}|$ are strongly enhanced (i.e., about three times larger than the ones obtained in the standard nontotal reflection geometry), while the phase differences $\Delta\phi^{\alpha\beta}$ vary strongly through the resonance.

As we already discussed, the MO components $\Delta R^{\alpha\beta}$ are proportional to the product of the values of the two components orthogonal to the magnetization of the fields $\mathbf{e}_{21}^{s}(z_c)$ and $\mathbf{e}_{21}^{p}(z_c)$, calculated in the pure gold layer at the altitude z_c of the cobalt layer [Eq. (12)]. More precisely, for polar Kerr effect these field components are $e_{21}^{x}(z_c)$ and $e_{21}^{y}(z_c)$ while for longitudinal Kerr effect the relevant components are $e_{21}^{z}(z_c)$ and $e_{21}^{y}(z_c)$. As shown in curves (c) and (d) of Figs. 6 and 7, if the y (or s) component exhibits no particular feature in the variation of either its modulus or its phase, the x and z components show on the contrary a resonant feature at the incidence angle where the SP's are excited. The important point is that the observed variation of the MO components of the reflected light electric field (ΔR^{sp} and ΔR^{ps}),

in particular its resonant feature, directly images the variation of the value at the Co layer of the component of the p field involved in the MO Kerr effect, i.e., of $e_{21}^{x}(z_c)$ for polar geometry and of $e_{21}^{z}(z_c)$ for longitudinal geometry [compare curves (a) and (b) with curves (c) and (d) in Figs. 6 and 7].

Note that, while the theoretical fits in curves (a) and (b) of Figs. 6 and 7 (full lines) account for the losses in Co, the curves (c) and (d) in Figs. 6 and 7 are calculated for a pure gold film. This shows that the SP resonance is not very much affected by the presence of the Co layer and that therefore, in such thin ferromagnetic films, one can make full profit of the resonant enhancement effect (see the Appendix).

2. Equatorial MO effect

The equatorial MO Kerr effect is an intensity effect which corresponds to the difference $\Delta\mathcal{R}_I$ of reflected intensity, for a p-polarized light, between the two opposite magnetization states of a ferromagnet with in-plane easy magnetization axis perpendicular to the incidence plane (here along the y axis):

$$\Delta\mathcal{R}_I = 2\,\mathrm{Re}(R^{0p}\overline{\Delta R^{pp}}), \tag{18}$$

where R^{0p} is the reflected p field for zero magnetization.
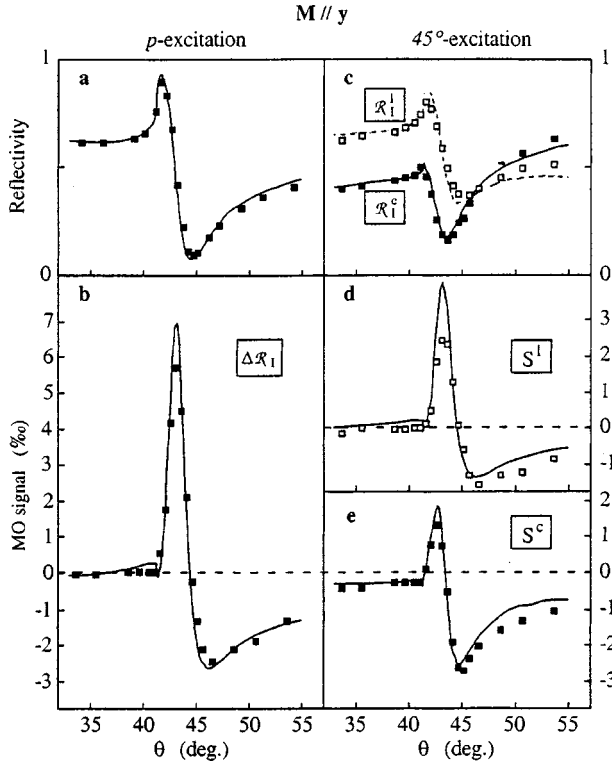
FIG. 8. Variation with the incidence angle θ of the reflectivity $\mathcal{R}_I$ (curve a) and of the usual intensity MO response $\Delta\mathcal{R}_I$ (curve b), in the equatorial ($\mathbf{M}\|\mathbf{y}$) configuration, measured on sample 2 for a p excitation. Variation with θ of the $\mathcal{R}_I^l$ and $\mathcal{R}_I^c$ (curves c, symbols $\square$ and $\blacksquare$, respectively) and of the equatorial ($\mathbf{M}\|\mathbf{y}$) MO responses S^l and S^c (curves d and e) measured, for an incident polarization rotated by $45°$ from the s- and p-polarization directions, respectively with a linear and a circular analyzer. The symbols correspond to the measurements, the full and dotted lines represent the theoretical fits.

We have measured, versus the incidence angle, the mean reflected intensity $\mathcal{R}_I$ [Fig. 8(a)] and the equatorial MO response $\Delta\mathcal{R}_I$ of sample 2 [Fig. 8(b)]. The $\mathcal{R}_I$ curve is obviously very similar to the one obtained in the longitudinal geometry. In the nontotal reflection range of incidence angles ($\theta < \theta_c$), the value of the MO signal, which is anyway not expected to be very large, is almost zero in the particular case of sample 2. But beyond θ_c, $\Delta\mathcal{R}_I$ exhibits a huge peak in the SP region.

In order to achieve a complete analysis of the equatorial MO effect, we have performed MO measurements in an unusual geometry where the linear excitation polarization is rotated at $45°$ from the s (and p) axis and where a polarization analyzer (linear or circular) is introduced in front of the detector. In these conditions, when using a linear analyzer, the measured reflected intensity $\mathcal{R}_I^l$ [open squares in Fig. 8(c)] and the MO response S^l [Fig. 8(d)], are given by[17]

$$\mathcal{R}_I^l = \frac{|R^{0p} - R^{0s}|^2}{4}, \qquad (19)$$

$$S^l = \text{Re}[R^{0p}\overline{\Delta R^{pp}}] - \text{Re}[R^{0s}\overline{\Delta R^{pp}}]. \qquad (20)$$
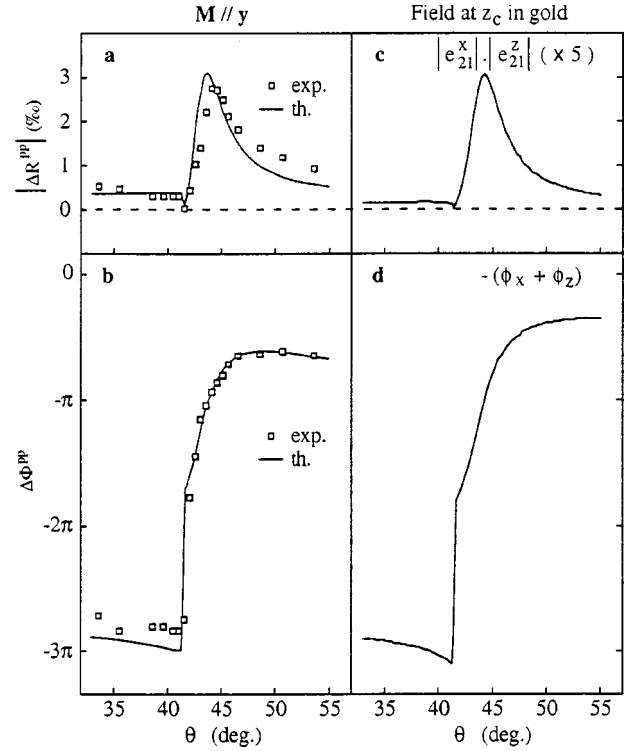
FIG. 9. Variation with θ of $|\Delta R^{pp}|$ (curve a), the amplitude of ΔR^{pp}, the equatorial MO figure of merit, and of $\Delta\Phi^{pp}$ (curve b), the phase difference between ΔR^{pp} and R^{0s}. Variation with θ of the amplitude (curve c) and phase (curve d) of the product of $e_{21}^x(z_c)$ and $e_{21}^z(z_c)$, the two p components of the field in a pure gold film (for a unit p excitation) at the location of the Co layer center.

When using a circular analyzer, the measured reflected intensity $\mathcal{R}_I^c$ [closed squares in Fig. 8(c)], and the MO response, S^c [Fig. 8(e)], are given by

$$\mathcal{R}_I^c = \frac{|R^{0p} + iR^{0s}|^2}{4}, \qquad (21)$$

$$S^c = \text{Re}(R^{0p}\overline{\Delta R^{pp}}) + \text{Im}(R^{0s}\overline{\Delta R^{pp}}). \qquad (22)$$

With both polarization analyzers, the reflectivity and the MO signal show a feature related to the SP resonance. From the measurements of S^l, S^c, $\Delta\mathcal{R}_I$, and using the experimental variation of R^{0s} [deduced from Fig. 5(g)] we have determined the variation with θ of the MO component ΔR^{pp} of the equatorial MO effect, or more precisely of $|\Delta R^{pp}|$ [Fig. 9(a)] and of $\Delta\phi^{ps}$ the phase difference between ΔR^{pp} and R^{0s} [Fig. 9(b)]. Around θ_R, ΔR^{pp} exhibits a very sharp resonant feature: $|\Delta R^{pp}|$ is enhanced by nearly a factor 10 when compared to the value measured in the usual nontotal reflection configuration (i.e., for $\theta < \theta_c$) and $\Delta\phi^{ps}$ (which almost varies similar to the ΔR^{pp} phase) jumps by about 2π. Moreover, at resonance, $|\Delta R^{pp}|$ is about four times larger than $|\Delta R^{ps}|$ [Fig. 7(a)] the MO component measured on the same sample in the longitudinal Kerr geometry while, for $\theta < \theta_c$, $|\Delta R^{pp}|$ is only two times larger than $|\Delta R^{ps}|$.

This stronger enhancement of the MO component $|\Delta R^{pp}|$ at resonance is related to the fact that in the equatorial Kerr

effect both the excitation field and the MO component are p waves and therefore couple with the SP modes. In other words, the two components of the field coupled through the equatorial MO effect are the x and z components. Then, according to Eq. (15), the MO component of the reflected field is proportional to the product of the two components of the p field at the location of the Co layer $e_{21}^x(z_c)$ and $e_{21}^z(z_c)$. As shown in Figs. 6(c) and 7(c), these components are both enhanced at θ_R as the resonant factor r_{23}^p appears in their expressions [Eq. (8b)], and therefore their product superimposes these enhancement effects (Fig. 9, curves c and d). Here again, when comparing curves a and b with curves c and d in Fig. 9, it is clear that the MO component ΔR^{pp} directly images the product of the values at the Co layer of $e_{21}^x(z_c)$ and $e_{21}^z(z_c)$ the electric field components involved in the MO effect, and therefore reproduces the related resonant feature.

B. Rotation and ellipticity, figure of merit, and signal-to-noise ratio

The most commonly discussed MO quantities are the Kerr (or Faraday) rotation and ellipticity that we note here, respectively, K^l and K^c. They are defined in the polar and longitudinal geometries as

$$K^l \approx \tan(K^1) = \frac{S^l}{2\mathcal{R}_I} \quad \text{and} \quad K^c \approx \tan(K^c) = \frac{S^c}{2\mathcal{R}_I}. \quad (23)$$

However, considering these quantities can be misleading for a quantitative analysis of the MO properties of a system. Indeed, as evidenced when writing K^l and K^c as a function of the quantities that we discussed in the previous section (namely, R^{0s}, ΔR^{ps}, and $\Delta \phi^{ps}$ or R^{0p}, ΔR^{sp}, and $\Delta \phi^{sp}$), any approach to enhance the MO response of a structure including a given magnetic material must fulfill two conditions: the medium must provide a large Kerr rotation (or ellipticity) and a high reflectivity.[1,3]

In Fig. 10, the polar Kerr rotation (curves b and e) and ellipticity (curves c and f) deduced from the measurements presented in Fig. 5 are plotted as a function of the incidence angle. At resonance, for both s and p excitations, the ellipticity goes through zero and the Kerr rotation is strongly enhanced when compared to the value measured in the non-total reflection range. Nevertheless, this resonant enhancement effect reaches about a factor 10 for p excitation, and a factor 3 for s excitation. This difference between the two incident polarizations is in fact "artificial": it is not due to the MO properties of the system but features the variation of the reflectivity. Indeed, as can be seen from curve b in Fig. 5, the reflectivity $\mathcal{R}_I$, which enters as a denominator in the expression of K^l for p excitation goes through a deep minimum (close to zero) at resonance. On the contrary, for s excitation, because the reflectivity (see curve a in Fig. 5) does not show any particular feature and remains almost equal to 1 in the whole range of incidence angle, the enhancement (by a factor 3) of K^l at θ_R is directly related to the one of $|\Delta R^{ps}|$ [Fig. 6(a)]. This emphasizes that when the reflectivity varies (which is for instance the case near the plasma edge),[2] the Kerr rotation and ellipticity are not suffi-
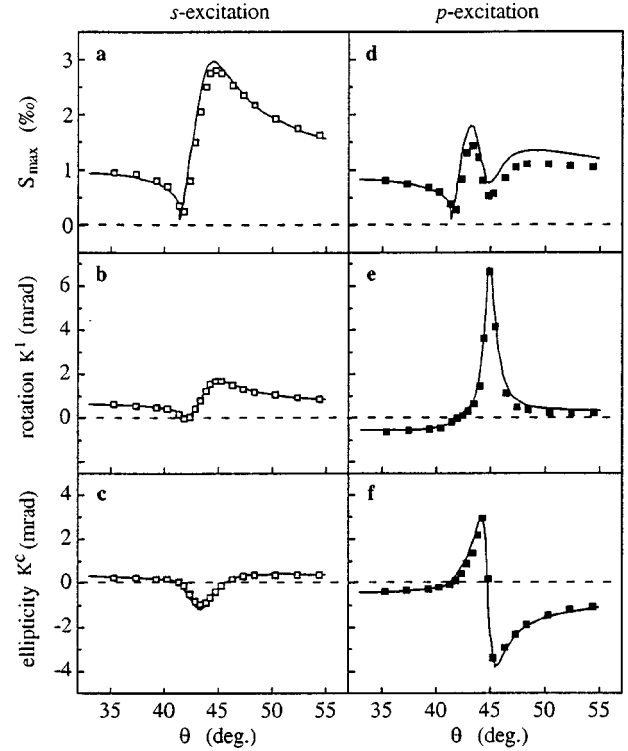
FIG. 10. In the polar configuration (**M**∥**z**), polar Kerr rotation (curves b and e), polar Kerr elipticity (curves c and f) and maximum polar MO response (curves a and d) as a function of the incidence angle θ, for s (left column) and p (right column) excitations. The symbols represent the experimental points and the full lines are obtained from theory.

cient to describe the MO properties of the system, and an increase of these quantities may not be significant.

In fact, the relevant MO quantity is the modulus of the MO component of the reflected light electric field ($|\Delta R^{ps}|$ for s excitation and $|\Delta R^{sp}|$ for p excitation) which is usually taken as the MO figure of merit.[3,18] Indeed, in the limit where the noise is dominated by the shot noise (i.e., is proportional to $|R^{0s}|$ or $|R^{0p}|$, the square root of the reflectivity), the signal-to-noise ratio related to the measurement of the MO response is proportional to $|\Delta R^{ps}|$ or $|\Delta R^{sp}|$ as can be obviously seen from Eqs. (16) and (17). These quantities, which are independent of the reflectivity, are identical for both s and p incident polarizations and show a large enhancement when the SP's are excited [Figs. 6(a) and 7(a)].

On another respect, the maximum MO response $S^{\max} = [(S^l)^2 + (S^c)^2]^{1/2}$ (Fig. 10 curves a and d) can be deduced from the measurements presented in Fig. 5, or directly measured by compensating at detection the phase difference ($\Delta \phi^{ps}$ or $\Delta \phi^{sp}$) between the s and p components of the reflected light electric field. At resonance, for both s and p excitations, S^c (i.e., the ellipticity) goes through zero (curves c and f in Fig. 10) and $S^{\max}$ is almost equal to S^l. But for p excitation $S^{\max}$ is quite small at θ_R [Fig. 10(d)] because the resonant behavior of $|\Delta R^{sp}|$ is attenuated by the vanishing reflection coefficient $|R^{0p}|$, while for s excitation, as $|R^{0s}|$ is almost equal to unity, the variation of $S^{\max}$ [Fig. 10(a)] reproduces the resonant enhancement of $|\Delta R^{sp}|$. The highest
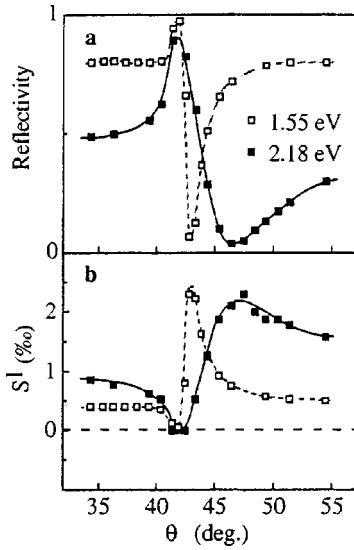
FIG. 11. In the polar configuration (**M**∥**z**), variation with θ of the reflectivity for p excitation (curves a) and of the polar MO response S^l for s excitation (curves b) measured on sample 1 for two values of the excitation energy ($\hbar\omega = 1.55$ eV and $\hbar\omega = 2.18$ eV).

reflectivity for s excitation yields a highest MO signal: this provides a "perfect amplification" effect which does not occur with p excitation.

Therefore, in noble-metal–ferromagnetic-metal multilayer thin films the three conditions required to obtain a high MO response with a high signal-to-noise ratio (large rotation, zero ellipticity, and high reflectivity) are satisfied for s excitation at the noble metal SP resonance. Although the Kerr rotation is larger at resonance for p excitation than for s excitation, the figure of merit, i.e., the signal-to-noise ratio, is identical for both incident polarizations ($|\Delta R^{ps}| = |\Delta R^{sp}|$), and the use of a s excitation even provides an additional "perfect amplification" effect due to a high reflectivity.

Note that, in the longitudinal and equatorial configurations, the figures of merit are, respectively, ΔR^{sp}, (ΔR^{ps}), and ΔR^{pp}. When comparing these quantities one sees that, in the same system (here sample 2), the MO figure of merit is larger in the equatorial configuration than in the longitudinal geometry: four times larger at resonance and about two times larger off resonance for $\theta < \theta_c$. Therefore, in the case of samples with in-plane magnetization, using the excitation and detection conditions of our equatorial MO experiment (or any other similar conditions) can have significant advantages when compared to the usual longitudinal geometry.

C. Spectral dependence of surface enhanced magneto-optics

One of the main advantages of SP's over most of the other MO effect enhancement mechanisms is the possibility to achieve this resonant excitation in a wide spectral range. Indeed, it can be seen from the dispersion relation of the SP's (Fig. 1) that the coupling with photons of a given energy is simply obtained by tuning the value of the incidence angle θ. In Fig. 11(a), we have plotted the variation with incidence angle of the reflectivity of a p-polarized incident light mea-
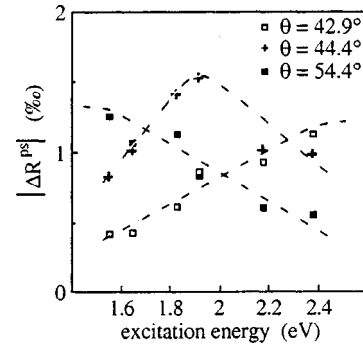
FIG. 12. In the polar configuration (**M**∥**z**), variation with $\hbar\omega$ of $|\Delta R^{ps}|$ for three different values of θ larger than θ_c.

sured on sample 1 for two different values of the excitation energy: an infrared line ($\hbar\omega = 1.55$ eV) and a yellow line ($\hbar\omega = 2.18$ eV) of the krypton-ion laser. The minimum of reflectivity, characteristic of the excitation of the SP resonance, is observed for these two light wavelengths at different values of the resonance angle θ_R: respectively, 43° and 47°. According to the dispersion relation of SP's, the larger the photon energy, the larger the value of θ_R. For the two photon energies, the enhancement effect on the polar MO response is observed at the corresponding resonance angle [Fig. 11(b)].

Conversely, we have measured the polar MO response of the system for three different values of the incident angle as a function of the excitation energy (Fig. 12). For the smallest value of the incident angle $\theta = 42.9°$, the resonant coupling is achieved in the near infrared range and the MO signal decreases with increasing photon energy. For the intermediate value of $\theta = 44.4°$, the resonance occurs for red light. At the corresponding wavelength, the MO response goes through a maximum. For the largest value of $\theta = 54.4°$, the resonance is shifted towards the blue side of the spectrum and the MO response increases with increasing photon energy.

The efficiency of the SP enhancement effect on the MO response depends on the resonance quality factor i.e., on the value of $|\varepsilon'_2/\varepsilon''_2|$: as shown in Sec. II, when the SP's are excited, the resonant factor r^p_{23} is approximately equal to $-4i\varepsilon'_2/\varepsilon''_2$. In noble metals, $|\varepsilon'_2/\varepsilon''_2|$ is very large for infrared frequencies where surface plasmons tend to a photonlike behavior, and diminishes with increasing energy. This explains the sharpness of the resonant feature in the reflectivity of a p-incident wave and in the MO response measured with $\hbar\omega = 1.55$ eV when compared to the broad equivalent peaks obtained with $\hbar\omega = 2.18$ eV (Fig. 12).

We have measured, versus the excitation energy, the variation of $|\Delta R^{ps}|$, the MO component modulus for s excitation, at resonance ($\theta = \theta_R$ is different for each $\hbar\omega$ value) and out of resonance at $\theta = 35°$, which is comparable with the usual "normal incidence" geometry [Fig. 13(a)]. No particular feature is observed in these smooth variations which are determined by the dependence on $\hbar\omega$ of all the optical constants involved in the problem. The enhancement of the MO figure of merit all over the probed spectral range appears clearly, as the value of $|\Delta R^{ps}|$ is always much larger at resonance than out of resonance. The ratio of the values of
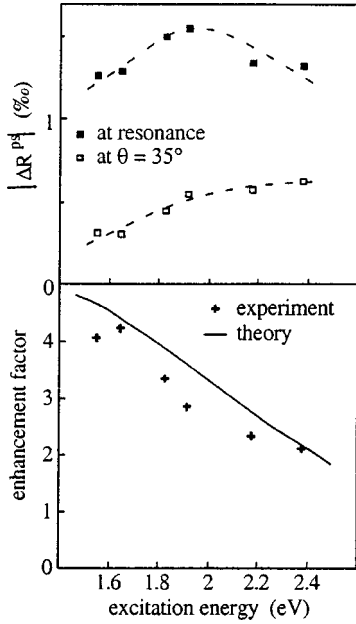
FIG. 13. In the polar configuration ($\mathbf{M}\|\mathbf{z}$), variation with excitation energy of $|\Delta R^{ps}|$ measured at resonance (symbols ■) and out of resonance in the nontotal reflection condition at $\theta = 35°$ (symbols □). Variation with $\hbar\omega$ of the related resonance enhancement factor $|\Delta R^{ps}(\theta_R)|/|\Delta R^{ps}(35°)|$ (symbols +).

$|\Delta R^{ps}|$ in these two regions gives the resonance enhancement factor which in fact characterizes the efficiency of the enhancement effect and depends almost only on the gold optical constants. As shown in Fig. 13(b), this enhancement factor decreases with increasing energy as expected from the variation of the SP resonance quality factor. In the near-infrared range, $|\Delta R^{ps}|$ is enhanced by almost a factor of 5 and when increasing the photon energy, the enhancement reduces but still remains close to 3 for green light. This variation is in reasonable agreement with the theoretical curve [full line in Fig. 13(b)] calculated after the treatment described in Sec. II and in the Appendix, and only taking into account the variation with $\hbar\omega$ of the dielectric function of gold ε_2 taken from Ref. 15.

V. CONCLUSION

We have shown that in magnetic metallic multilayer systems the coupling of light with the SP modes may provide surface-enhanced MO effects. This coupling occurs in a very simple total reflection arrangement. We have presented a detailed experimental and theoretical investigation of the resonance effect of SP's on the MO properties of a Au/Co/Au model system. The results demonstrate that the conditions required to obtain a high MO response are satisfied at resonance, where a strong enhancement of the figure of merit (i.e., of the signal-to-noise ratio) is observed. This effect is directly related to the enhancement of the p components of the field at the location of the cobalt layer inside the gold thin film. The surface-enhanced MO effect occurs for any orientation of the easy-magnetization axis and is particularly important in the equatorial Kerr geometry. When varying the

photon energy, the efficiency of the enhancement of the MO figure of merit follows the variation of the quality factor of the SP resonance. The quality factor of the SP resonance is high when $|\varepsilon_2'/\varepsilon_2''| \gg 1$ which is the case for noble metals in a wide spectral range including the near infrared and visible domains. Therefore, this technique is particularly well adapted to noble-metal–ferromagnetic-metal multilayer structures, already known to exhibit large MO response in standard nontotal reflection geometry.

Other systems such as Pt/Co/Pt or Pd/Co/Pd, which receive a lot of attention, are not as good candidates for surface enhanced magneto-optics. Indeed, the ratio $|\varepsilon_2'/\varepsilon_2''|$ is only of about 0.6 for platinum and 1 for palladium (one order of magnitude smaller than for silver and gold) over the whole near-infrared and visible range. For these systems, the surface plasmon resonance is damped and cannot provide a significant enhancement of the MO figure of merit.

Finally, SP resonance in noble metals provides an electromagnetic enhancement mechanism which has already been successfully applied to the near-field MO response[5] and to the MO second harmonic generation[19] in magnetic metallic multilayer thin films.

APPENDIX: PERTURBATION OF THE GOLD HOST MATRIX OPTICAL PROPERTIES BY THE Co LAYER

As demonstrated in Chap. VI of Ref. 12, the optical response of a Au/Co/Au structure of total thickness d can be calculated by considering the thin Co layer of thickness ℓ as a perturbation of the gold host layer of same thickness d.

For instance, for a α-polarized light ($\alpha = s$ or p), the reflectivity of the Au/Co/Au structure $R^{0\alpha}$ (neglecting the MO effect) can be written as a function of the reflection and transmission coefficients of the pure gold layer R_{Au}^{α} and T_{Au}^{α}:

$$R^{0\alpha} \approx R_{Au}^{\alpha}\left(1 + \frac{\delta R^{\alpha}/R_{Au}^{\alpha}}{(1 - \delta T^{\alpha}/T_{Au}^{\alpha})}\right), \qquad (A1)$$

where δR^{α} and δT^{α} are defined by

$$\delta R^{\alpha} = \frac{ik_0^2\ell}{2\kappa_1}\overline{\mathbf{e}}_{21}^{\alpha}(z_c)[\underline{\eta}\cdot\mathbf{e}_{21}^{\alpha}(z_c)], \qquad (A2a)$$

$$\delta T^{\alpha} = \frac{ik_0^2\ell}{2\kappa_3}\overline{\mathbf{e}}_{23}^{\alpha}(z_c)[\underline{\eta}\cdot\mathbf{e}_{21}^{\alpha}(z_c)]. \qquad (A2b)$$

$\mathbf{e}_{23}^{\alpha}$ is the field in the gold layer calculated [from Eq. (8), replacing the index 1 by 3] for an incidence from medium 3 with the same in-plane wave-vector component θ. The vectors $\overline{\mathbf{e}}_{21}^{\alpha}$ and $\overline{\mathbf{e}}_{23}^{\alpha}$ are symmetric with respect to the plane yOz of the fields $\mathbf{e}_{21}^{\alpha}$ and $\mathbf{e}_{23}^{\alpha}$. The $\underline{\eta}$ matrix describes the continuity relations of the electromagnetic field in the z direction:

$$\underline{\eta} = (\varepsilon_m - \varepsilon_2)\begin{pmatrix} 1 & 0 & 0 \\ 0 & 1 & 0 \\ 0 & 0 & \varepsilon_m/\varepsilon_2 \end{pmatrix}. \qquad (A3)$$
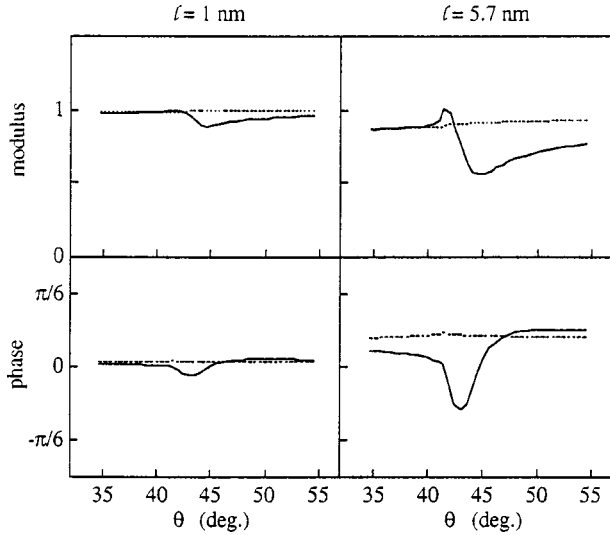
FIG. 14. (a) Variation with θ of the modulus and phase of the quantity $(1 - \delta T^{\alpha}/T^{\alpha}_{Au})^{-1}$, for the two linear polarizations $\alpha = s$ (dotted lines) and $\alpha = p$ (full lines) and for the two samples (sample 1 with a Co layer of thickness $\ell = 1$ nm and sample 2 with a Co layer of thickness $\ell = 5.7$ nm).

For s and p polarizations, it can be shown that

$$\frac{\delta T^s}{T^s_{Au}} = \frac{ik_0^2 \ell (\varepsilon_m - \varepsilon_2)}{2\kappa_2 t^s_{12}}$$

$$\times [\exp(i\kappa_2 z_c) + r^s_{21} \exp(-i\kappa_2 z_c)] e^s_{21}(z_c),$$

$$(A4a)$$

$$\frac{\delta T^p}{T^p_{Au}} = \frac{ik_0^2 \ell (\varepsilon_m - \varepsilon_2)}{2\kappa_2 t^p_{12}} \left\{ [\exp(i\kappa_2 z_c) - r^p_{21} \exp(-i\kappa_2 z_c)] \frac{\kappa_2}{k_2} \mathbf{x} \right.$$

$$\left. - [\exp(i\kappa_2 z_c) + r^p_{21} \exp(-i\kappa_2 z_c)] \frac{q}{k_2} \mathbf{z} \right\} [\underline{\eta} \cdot \mathbf{e}^p_{21}(z_c)].$$

$$(A4b)$$

The variation with incident angle of $\delta T^{\alpha}/T^{\alpha}_{Au}$ mainly follows that of the electric field in the gold layer $\mathbf{e}^{\alpha}_{21}(z_c)$.

It is also shown in Ref. 12 that the unperturbed field in cobalt $\mathbf{e}^{0\alpha}_{m1}$, which appears in the expression of the MO reflection coefficients $\Delta R^{\alpha\beta}$ [Eq. (12) of the main text], is related to the field in a pure gold film $\mathbf{e}^{\alpha}_{21}(z_c)$, by the quantity $(1 - \delta T^{\alpha}/T^{\alpha}_{Au})^{-1}$ [Eq. (11) of the main text]:

$$\mathbf{e}^{0\alpha}_{m1} = \frac{\mathbf{e}^{\alpha}_{21}(z_c)}{1 - \delta T^{\alpha}/T^{\alpha}_{Au}}.$$

$$(A5)$$

The modulus and phase of the quantity $(1 - \delta T^{\alpha}/T^{\alpha}_{Au})^{-1}$ are plotted in Fig. 14 for the two systems experimentally studied and for the s and p polarizations. This quantity does not differ very much from unity over the probed incidence angle range except by a small extra damping feature for p waves in the vicinity of the SP resonance

Consequently, the quantity $R^{0\alpha}/R^{\alpha}_{Au}$ is also close to unity. The reflectivity of the Au/Co/Au system is therefore very similar to that of the pure gold layer. In this case, the small damping feature almost only changes the width of the SP dip in the p reflectivity.

---

*Permanent address: A. F. Ioffe Physico-Technical Institute, 194021 Saint-Petersburg, Russia.

†Permanent address: Groupe de Physique de l'Etat Condensé, UMR 6631-CNRS, Université de la Méditerranée, Faculté des Sciences de Luminy, Département de Physique, 13288 Marseille Cedex 9-France.

[1] R. Atkinson, I. W. Salter, and J. Xu, J. Magn. Magn. Mater. **102**, 357 (1991); R. Atkinson, *ibid.* **124**, 178 (1993).

[2] T. Katayama, Y. Suzuki, H. Awano, Y. Nishihara, and N. Koshizuka, Phys. Rev. Lett. **60**, 1426 (1988); W. A. McGahan, L.-Y. Chen, Z. S. Shan, D. J. Sellmyer, and J. A. Woollam, Appl. Phys. Lett. **55**, 2479 (1989); J. Ferré, *Proceedings of the Conference on Magnetism, Magnetic Materials and Their Applications*, La Habana, Cuba, 1991, edited by F. Leccabue and J. L. Sanchez Llamazares (IOP Publishing, Bristol, 1992), p. 167.

[3] W. Reim and D. Weller, IEEE Trans. Magn. **25**, 3752 (1989).

[4] *Surface Enhanced Raman Scattering*, edited by R. K. Chang and T. E. Furnak (Plenum Press, New York, 1982).

[5] V. I. Safarov, V. A. Kosobukin, C. Hermann, G. Lampel, J. Peretti, and C. Marlière, Phys. Rev. Lett. **73**, 3584 (1994).

[6] V. A. Kosobukin, Solid State Commun. **101**, 497 (1997).

[7] H. Raether, *Surface Plasmons*, in Vol. 11 of *Springer Tracts in Modern Physics* (Springer Verlag, 1988); H. Raether, in *Surface Polaritons*, edited by V. M. Agranovich and D. L. Mills (North Holland, Amsterdam, 1982), p. 331.

[8] V. M. Agranovich, in *Surface Polaritons* (Ref. 7), p. 187.

[9] F. Abelès and T. Lopez-Rios, in *Surface Polaritons* (Ref. 7), p. 239.

[10] P. E. Fergusson, O. M. Stafsudd, and R. F. Wallis, Physica B **89**, 91 (1977).

[11] E. Kretschmann and H. Raether, Z. Naturforsch. A **23**, 2135 (1968); E. Kretschmann, Z. Phys. **241**, 313 (1971).

[12] P. Bertrand, C. Hermann, G. Lampel, J. Peretti, and V. I. Safarov, Phys. Rev. B **64**, 235421 (2001).

[13] C. Marlière, D. Renard, and J. P. Chauvineau, Thin Solid Films **201**, 317 (1991), and references therein.

[14] S. Visnovsky, M. Nyvlt, V. Prosser, J. Ferré, G. Pénissard, D. Renard, and G. Sczigel, J. Magn. Magn. Mater. **128**, 179 (1993).

[15] P. B. Johnson and R. W. Christy, Phys. Rev. B **6**, 4370 (1972).

[16] P. B. Johnson and R. W. Christy, Phys. Rev. B **9**, 5056 (1973).

[17] For these measurements, the linear analyzer is oriented at 45° from the s- and p-polarization directions. Two orientations (at 90° one from the other) of the axis of the linear analyzer are then possible. The one we have chosen corresponds to Eqs. (19) and (20). The measurements with the other orientation, which allow the same analysis, are described by similar equations in which the difference $R^{0p} - R^{0s}$ is changed into the sum $R^{0p} + R^{0s}$.

[18] E. R. Moog, J. Zak, and S. D. Bader, J. Appl. Phys. **69**, 880 (1991).

[19] V. V. Pavlov, G. Tessier, C. Malouin, P. Georges, A. Brun, D. Renard, P. Meyer, J. Ferré, and P. Beauvillain, Appl. Phys. Lett. **75**, 190 (1999).